


Nature of intermediate magnetization plateaus of a spin-1/2 Ising-Heisenberg model on a triangulated Husimi lattice resembling a triangulated kagome lattice

Jozef Strečka^{1,*} and Cesur Ekiz^{2,†}

¹*Department of Theoretical Physics and Astrophysics, Faculty of Science, P. J. Šafárik University, Park Angelinum 9, 040 01 Košice, Slovak Republic*

²*Department of Physics, Faculty of Science and Letter, Aydın Adnan Menderes University, 09010 Aydın, Turkey*

 (Received 6 March 2020; accepted 28 June 2020; published 14 July 2020)

The spin-1/2 Ising-Heisenberg model on a triangulated Husimi lattice is exactly solved in a magnetic field within the framework of the generalized star-triangle transformation and the method of exact recursion relations. The generalized star-triangle transformation establishes an exact mapping correspondence with the effective spin-1/2 Ising model on a triangular Husimi lattice with a temperature-dependent field, pair and triplet interactions, which is subsequently rigorously treated by making use of exact recursion relations. The ground-state phase diagram of a spin-1/2 Ising-Heisenberg model on a triangulated Husimi lattice, which bears a close resemblance with a triangulated kagomé lattice, involves, in total, two classical and three quantum ground states manifested in respective low-temperature magnetization curves as intermediate plateaus at 1/9, 1/3, and 5/9 of the saturation magnetization. It is verified that the fractional magnetization plateaus of quantum nature have character of either dimerized or trimerized ground states. A low-temperature magnetization curve of the spin-1/2 Ising-Heisenberg model on a triangulated Husimi lattice resembling a triangulated kagome lattice may exhibit either no intermediate plateau, a single 1/3 plateau, a single 5/9 plateau, or a sequence of 1/9, 1/3, and 5/9 plateaus depending on a character and relative size of two considered coupling constants.

DOI: [10.1103/PhysRevE.102.012132](https://doi.org/10.1103/PhysRevE.102.012132)

I. INTRODUCTION

A rigorous solution of two-dimensional frustrated Heisenberg spin models by state-of-the-art analytical and numerical techniques represents a challenging topic of modern statistical physics with regard to an outstanding diversity of their low-temperature magnetic behavior closely related to nonnegligible effect of quantum fluctuations [1–4]. The geometric spin frustration is frequently indispensable for an observation of fractional quantized plateaus in low-temperature magnetization curves of two-dimensional Heisenberg spin models, which appear as a direct consequence of field-driven stabilization of often peculiar quantum ground states with a finite energy gap in a respective excitation spectrum [5–7]. It should be pointed out, moreover, that theoretical predictions of several exotic quantum ground states have already been experimentally testified by high-field measurements performed on a few paradigmatic prototypes of two-dimensional quantum spin models, such as a Shastry-Sutherland compound $\text{SrCu}(\text{BO}_3)_2$ [8–12], a triangular-lattice compound Cs_2CuBr_4 [13,14] or kagome-lattice compounds $\text{Cu}_3(\text{titmb})_2(\text{OCOCH}_3)_6$ [15] and $\text{CdCu}_3(\text{OH})_6(\text{NO}_3)_2$ [16].

Bearing this in mind, it appears worthwhile to investigate the microscopic nature of intriguing quantum ground states emergent in low-temperature magnetization curves of two-dimensional frustrated Heisenberg spin systems as interme-

mediate plateaus at fractional values of the saturation magnetization. A subtle nature of quantum ground states, however, necessitates application of nonperturbative (at best, exact analytical or numerical) approaches, which are mostly inapplicable to two-dimensional frustrated quantum Heisenberg spin models due to insurmountable computational complexities [1–4]. Recently, the numerical tensor-network methods were employed in order to study a geometric frustration of the quantum Heisenberg spin models on the Husimi lattice, which refers to a deep interior of recursive tree built up from interconnected polygons [17]. Compared to this, the method of exact recursion relations [18–21] offers a substantial simplification of a rigorous treatment of the frustrated Ising spin models defined on the Husimi lattices [22–32]. It should be pointed out, moreover, that this rigorous method in combination with algebraic mapping transformations can be straightforwardly adapted in order to obtain exact solutions for the frustrated Ising-Heisenberg models composed of classical Ising and quantum Heisenberg spins, which are valid also at nonzero temperatures and magnetic fields [33–36].

In the present paper, we will exactly solve the spin-1/2 Ising-Heisenberg model on a triangulated Husimi lattice, which bears a close resemblance with the triangulated kagome lattice as the underlying magnetic lattice of a series of polymeric coordination compounds $\text{Cu}_9\text{X}_2(\text{cpa})_6 \cdot n\text{H}_2\text{O}$ (cpa = carboxypentonic acid; $X = \text{F}, \text{Cl}, \text{Br}$) [37–39]. The magnetic compounds $\text{Cu}_9\text{X}_2(\text{cpa})_6 \cdot n\text{H}_2\text{O}$ belong to a prominent class of highly frustrated materials with no spontaneous magnetic orderings down to 1.7 K [40,41] and a striking intermediate plateau around 1/3 of the saturation magnetization in a

*jozef.strecka@upjs.sk

†cekiz@adu.edu.tr

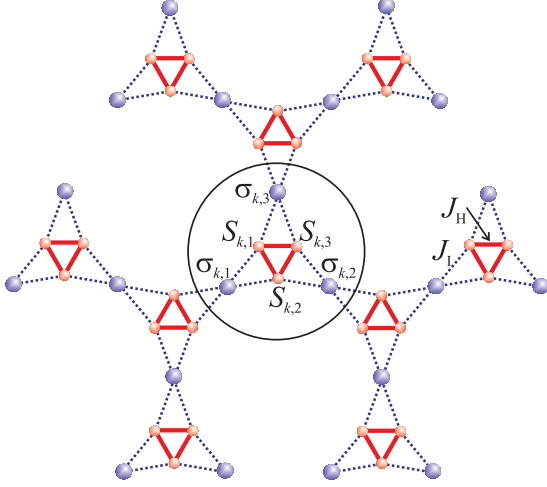


FIG. 1. A schematic illustration of the spin-1/2 Ising-Heisenberg model on a triangulated Husimi lattice with the ramification number $q = 2$. Small and large spheres denote lattice positions of the Heisenberg and Ising spins, respectively. The Heisenberg coupling J_H is schematically represented by solid lines, whereas the Ising coupling J_I is shown by dotted lines. A circle delimits the k th triangle-in-triangles unit described by the cluster Hamiltonian (3).

high-field magnetization curve [42,43]. Recent experimental measurements on magnetic compounds $\text{Cu}_9\text{X}_2(\text{cpa})_6 \cdot n\text{H}_2\text{O}$ additionally verified anomalous low-temperature thermodynamics [44,45] as well as the enhanced magnetocaloric effect [46,47].

It should be stressed that the spin-1/2 Ising-Heisenberg model on triangulated kagome [48,49], triangular [50,51], and Husimi [52,53] lattices have been exactly solved in a zero magnetic field, whereas the effect of nonzero magnetic fields has been comprehensively studied just for triangulated kagome [49] and triangular [51] lattices at absolute zero temperature yet. It has been convincingly evidenced in the previous studies [48–53] that the geometric frustration of the spin-1/2 Ising-Heisenberg model on the triangulated lattices is responsible either for a peculiar quantum long-range order or disorder at finite temperatures. For instance, the spin-1/2 Ising-Heisenberg model on a triangulated Husimi lattice exhibits, in a highly frustrated parameter region, a spontaneous long-range order or disorder depending on a size of the ramification number [52].

The outline of this paper is as follows. The spin-1/2 Ising-Heisenberg model on a triangulated Husimi lattice will be introduced in Sec. II together with a few basic steps of its exact treatment. The most interesting results for the ground-state and magnetization process will be thoroughly analyzed in Sec. III. A brief summary of the most important findings and the main conclusions are then summarized in Sec. IV.

II. MODEL AND METHOD

Let us consider the spin-1/2 Ising-Heisenberg model on a triangulated Husimi lattice to be further abbreviated as IHM-THL, which is schematically depicted in Fig. 1 for the particular choice of the ramification number $q = 2$. The

term triangulated Husimi lattice denotes a deep interior of a recursively built triangles-in-triangles Husimi tree, which consists of two different types of lattice sites schematically shown in Fig. 1 by large and small spheres, respectively. It is supposed that the lattice sites from all inner (outer) triangles of the triangulated Husimi lattice shown by small (large) spheres are occupied by the Heisenberg (Ising) spins. The total Hamiltonian of the IHM-THL in a presence of the external magnetic field can be accordingly defined as follows:

$$\hat{\mathcal{H}} = -J_H \sum_{(i,j)} \hat{\mathbf{S}}_i \cdot \hat{\mathbf{S}}_j - J_I \sum_{(j,k)} \hat{S}_j^z \hat{\sigma}_k^z - h_I \sum_{k=1}^N \hat{\sigma}_k^z - h_H \sum_{j=1}^{Nq} \hat{S}_j^z, \quad (1)$$

where $(\hat{\mathbf{S}}_i \cdot \hat{\mathbf{S}}_j) = \hat{S}_i^x \hat{S}_j^x + \hat{S}_i^y \hat{S}_j^y + \hat{S}_i^z \hat{S}_j^z$, \hat{S}_j^α ($\alpha = x, y, z$) and $\hat{\sigma}_k^z$ denote spatial components of the spin-1/2 operator assigned to the Heisenberg and Ising spins from the lattice sites forming inner and outer triangles of a triangulated Husimi lattice, respectively. The interaction term J_H labels the exchange interaction between the nearest-neighbor Heisenberg spins, the interaction term J_I denotes the Ising coupling between the nearest-neighbor Heisenberg and Ising spins, N denotes the total number of the Ising spins, and q is the ramification number that determines how many triangle-in-triangles units meet at each site of outer triangles. Finally, Zeeman's terms h_I and h_H account for the magnetostatic energy of the Ising and Heisenberg spins in a presence of the longitudinal magnetic field.

The total Hamiltonian (1) of the IHM-THL can be decomposed into a sum taken over the cluster Hamiltonians,

$$\hat{\mathcal{H}} = \sum_{k=1}^{Nq/3} \hat{\mathcal{H}}_k, \quad (2)$$

whereas each cluster Hamiltonian $\hat{\mathcal{H}}_k$ involves all interaction terms of three Heisenberg spins from the k th triangle-in-triangles unit (see Fig. 1) further referred to as the k th Heisenberg trimer,

$$\begin{aligned} \hat{\mathcal{H}}_k = & -J_H \sum_{i=1}^3 \vec{S}_{k,i} \cdot \vec{S}_{k,i+1} - J_I \sum_{i=1}^3 \hat{\sigma}_{k,i}^z (\hat{S}_{k,i}^z + \hat{S}_{k,i+1}^z) \\ & - h_H \sum_{i=1}^3 \hat{S}_{k,i}^z - \frac{h_I}{q} \sum_{i=1}^3 \hat{\sigma}_{k,i}^z. \end{aligned} \quad (3)$$

Note that the cyclic condition $S_{k,4} \equiv S_{k,1}$ is assumed in Eq. (3) and the factor $1/q$ at the last term ensures a correct counting of Zeeman's term h_I pertinent to the Ising spins, which is symmetrically split into q different cluster Hamiltonians of the triangle-in-triangles units sharing one and the same lattice site. Owing to a validity of the commutation relation between different cluster Hamiltonians $[\hat{\mathcal{H}}_i, \hat{\mathcal{H}}_j] = 0$, the partition function of the IHM-THL can be partially factorized into the following product:

$$\mathcal{Z} = \sum_{\{\sigma\}} \prod_{k=1}^{Nq/3} \text{Tr}_k \exp(-\beta \hat{\mathcal{H}}_k) = \sum_{\{\sigma\}} \prod_{k=1}^{Nq/3} \mathcal{Z}_k(\sigma_{k,1}^z, \sigma_{k,2}^z, \sigma_{k,3}^z), \quad (4)$$

where $\beta = 1/(k_B T)$, k_B is Boltzmann's constant, T is the absolute temperature, the symbol $\sum_{\{\sigma\}}$ denotes a summation

over all available configurations of the Ising spins, and the symbol $\text{Tr}_k = \text{Tr}_{S_{k,1}} \text{Tr}_{S_{k,2}} \text{Tr}_{S_{k,3}}$ stands for a trace over spin degrees of freedom of the k th Heisenberg trimer. The mathematical structure of Eq. (4) implies that one may perform a trace over spin degrees of freedom of different Heisenberg trimers independently of each other. If doing so, one gets an explicit form of Boltzmann's weight \mathcal{Z}_k , which exclusively depends just on the three Ising spins $\sigma_{k,1}$, $\sigma_{k,2}$, and $\sigma_{k,3}$ attached to the k th Heisenberg trimer. Subsequently, the effective Boltzmann's weight \mathcal{Z}_k can be replaced with an equivalent expression through the generalized star-triangle transformation [33–36],

$$\begin{aligned} \mathcal{Z}_k(\sigma_{k,1}^z, \sigma_{k,2}^z, \sigma_{k,3}^z) &= \text{Tr}_k \exp(-\beta \hat{\mathcal{H}}_k) \\ &= A \exp \left[\beta R_2 (\sigma_{k,1}^z \sigma_{k,2}^z + \sigma_{k,2}^z \sigma_{k,3}^z + \sigma_{k,3}^z \sigma_{k,1}^z) \right. \\ &\quad \left. + \beta R_3 \sigma_{k,1}^z \sigma_{k,2}^z \sigma_{k,3}^z + \frac{\beta R_1}{q} (\sigma_{k,1}^z + \sigma_{k,2}^z + \sigma_{k,3}^z) \right]. \end{aligned} \quad (5)$$

The star-triangle transformation represents, in fact, a set of eight algebraic equations, which can be obtained from the mapping relation (5) by substituting all available spin configurations of the three Ising spins $\sigma_{k,1}$, $\sigma_{k,2}$, and $\sigma_{k,3}$. Owing to the symmetry, one merely gets four independent equations explicitly given in Appendix A [see Eqs. (A1)–(A4)], which unambiguously determine yet unspecified mapping parameters A , R_1 , R_2 , and R_3 ,

$$A = (V_1 V_2 V_3 V_4^3)^{1/8}, \quad (6)$$

$$\beta R_1 = \beta h_l + \frac{q}{4} \ln \left(\frac{V_1 V_3}{V_2 V_4} \right), \quad (7)$$

$$\beta R_2 = \frac{1}{2} \ln \left(\frac{V_1 V_2}{V_3 V_4} \right), \quad (8)$$

$$\beta R_3 = \ln \left(\frac{V_1 V_4^3}{V_2 V_3^3} \right). \quad (9)$$

At this stage, one may directly substitute the star-triangle transformation (5) into the factorized form of the partition function (4) in order to get a rigorous mapping relationship,

$$\mathcal{Z}(\beta, J_l, J_H, h_l, h_H, q) = A^{Nq/3} \mathcal{Z}_{\text{eff}}(\beta, R_1, R_2, R_3, q), \quad (10)$$

which connects the partition function \mathcal{Z} of the IHM-THL with the partition function \mathcal{Z}_{eff} of the effective spin-1/2 Ising model on a triangular Husimi lattice schematically illustrated on the right-hand side of Fig. 2 and mathematically given by the Hamiltonian,

$$\mathcal{H}_{\text{eff}} = -R_2 \sum_{(i,j)} \sigma_i^z \sigma_j^z - R_3 \sum_{(i,j,k)} \sigma_i^z \sigma_j^z \sigma_k^z - R_1 \sum_{i=1}^N \sigma_i^z. \quad (11)$$

The first summation in Eq. (11) runs over the nearest-neighbor spin pairs, the second summation runs over the triangular unit cells, and, hence, the mapping parameters R_1 , R_2 and R_3 given by Eqs. (7)–(9) determine the effective field (R_1), the effective pair (R_2) and triplet (R_3) interactions of the corresponding spin-1/2 Ising model on a triangular Husimi

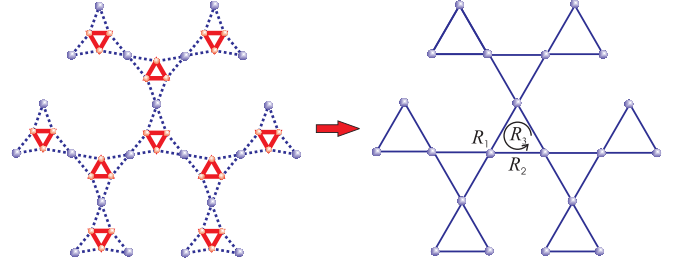


FIG. 2. The mapping correspondence between the IHM-THL and the effective spin-1/2 Ising model on a triangular Husimi lattice with the temperature-dependent field R_1 , the pair interaction R_2 , and the triplet interaction R_3 established by the star-triangle transformation (5).

lattice, whereas the mapping parameter A is just a simple multiplicative factor in the established mapping relation (10) between both partition functions. It is noteworthy that the similar mapping relation also holds between the Gibbs free energy G of the IHM-THL and the Gibbs free energy G_{eff} of the effective spin-1/2 Ising model on a triangular Husimi

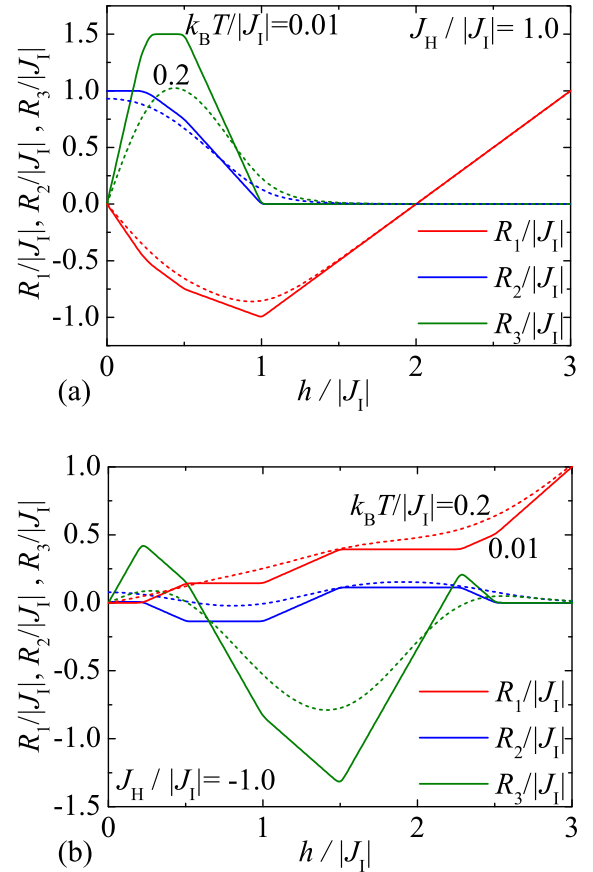


FIG. 3. The effective mapping parameters R_1 , R_2 , and R_3 versus magnetic field $h = h_l = h_H$ for the IHM-THL with the antiferromagnetic Ising coupling $J_l < 0$ and the ramification number $q = 2$ at two different temperatures $k_B T/|J_l| = 0.01$ (solid lines) and 0.2 (dotted lines). Two representative values of the Heisenberg interaction are considered: (a) $J_H/|J_l| = 1.0$ (ferromagnetic case); (b) $J_H/|J_l| = -1.0$ (antiferromagnetic case).

lattice,

$$G = -k_B T \ln \mathcal{Z} = G_{\text{eff}}(R_1, R_2, R_3) - \frac{Nqk_B T}{3} \ln A. \quad (12)$$

It should be pointed out that the mapping parameters R_1 , R_2 , and R_3 of the effective spin-1/2 Ising model on a triangular Husimi lattice basically depend on a magnetic field, interaction parameters, as well as temperature. For illustration, Fig. 3 depicts typical dependences of the effective mapping parameters R_1 , R_2 , and R_3 on a relative size of the magnetic field at two different temperatures and two selected values of the interaction ratio. It is quite clear from Fig. 3 that the magnetic field generally causes a highly nonmonotonous dependence of the effective interactions R_1 , R_2 , and R_3 , which may even change its character (sign) as, for instance, the effective pair and triplet interactions R_2 and R_3 plotted in Fig. 3(b). On the other hand, the rising temperature generally suppresses a relative strength of the mapping parameters R_1 , R_2 , and R_3 , which tend to zero in the asymptotic limit of the infinite temperature $T \rightarrow \infty$. Note, furthermore, that the effective field and triplet interaction R_1 and R_3 result from the action of the external magnetic field represented by the Hamiltonian parameters h_1 and h_H because both these mapping parameters tend to zero in the zero-field limit $h_1, h_H \rightarrow 0$.

In the following, our particular attention will be focused on a rigorous analysis of the magnetization process of the IHM-THL. To this end, it is necessary to calculate statistical

mean values determining the single-site magnetization of the Ising spins $m_I \equiv \langle \hat{\sigma}_k^z \rangle$ and the single-site magnetization of the Heisenberg spins $m_H \equiv \langle \hat{S}_k^z \rangle$. The single-site magnetization of the Ising spins can be calculated by differentiating the Gibbs free energy (12) with respect to the relevant magnetic field h_1 ,

$$m_I = -\frac{1}{N} \frac{\partial G}{\partial h_1} = -\frac{1}{N} \left(\frac{\partial G_{\text{eff}}}{\partial R_1} \right) \frac{\partial R_1}{\partial h_1} = m_{\text{eff}}(R_1, R_2, R_3). \quad (13)$$

According to Eq. (13), the single-site magnetization of the Ising spins of the IHM-THL directly equals the single-site magnetization of the spin-1/2 Ising model on a triangular Husimi lattice defined through the Hamiltonian (11) depending on the effective field R_1 , the effective pair interaction R_2 , and the effective triplet interaction R_3 as given by Eqs. (7)–(9). It should be pointed out, moreover, that the canonical ensemble average $m_{\text{eff}} \equiv \langle \hat{\sigma}_k^z \rangle_{\text{eff}}$ determining the single-site magnetization of the spin-1/2 Ising model on a triangular Husimi lattice defined through the Hamiltonian (11) can be rather easily calculated by the method of exact recursion relations [21] by following the same steps as previously used for a zero-field limit of the investigated model system [52],

$$m_{\text{eff}} \equiv \langle \sigma_k^z \rangle_{\text{eff}} = \frac{1}{2} \left[\frac{\exp(\beta R_1) - x^q}{\exp(\beta R_1) + x^q} \right], \quad (14)$$

whereas the quantity $x = \lim_{n \rightarrow \infty} x_n$ represents a stable fixed point of the recurrence relation,

$$x_n = \frac{\exp(2\beta R_1) + 2 \exp(\beta R_1 + \frac{\beta R_3}{4}) x_{n-1}^{q-1} + \exp(\beta R_2) x_{n-1}^{2q-2}}{\exp(2\beta R_1 + \beta R_2 + \frac{\beta R_3}{4}) + 2 \exp(\beta R_1) x_{n-1}^{q-1} + \exp(\frac{\beta R_3}{4}) x_{n-1}^{2q-2}}. \quad (15)$$

It could be, thus, concluded that magnetization of the effective spin-1/2 Ising model on a triangular Husimi lattice can be calculated from Eqs. (14) and (15) after solving the latter recursion relation iteratively. In view of the established mapping relation (13) between the magnetizations m_I and m_{eff} , the exact calculation of the single-site magnetization of the Ising spins of the IHM-THL is also completed.

On the other hand, the single-site magnetization of the Heisenberg spins $m_H \equiv \langle \hat{S}_k^z \rangle$ of the IHM-THL can be expressed in terms of the effective magnetization $m_{\text{eff}} \equiv \langle \sigma_k^z \rangle_{\text{eff}}$, the effective pair correlation function $\varepsilon_{\text{eff}} \equiv \langle \sigma_{k,1}^z \sigma_{k,2}^z \rangle_{\text{eff}}$ and the effective triplet correlation function $\tau_{\text{eff}} \equiv \langle \sigma_{k,1}^z \sigma_{k,2}^z \sigma_{k,3}^z \rangle_{\text{eff}}$ of the corresponding spin-1/2 Ising model on a triangular Husimi lattice,

$$\begin{aligned} m_H &= -\frac{1}{Nq} \frac{\partial G}{\partial h_H} \\ &= \frac{1}{3} \frac{\partial \ln A}{\partial \beta h_H} + \frac{m_I}{q} \frac{\partial R_1}{\partial h_H} + \varepsilon_{\text{eff}} \frac{\partial R_2}{\partial h_H} + \frac{\tau_{\text{eff}}}{3} \frac{\partial R_3}{\partial h_H}. \end{aligned} \quad (16)$$

A differentiation of the mapping parameters R_1 , R_2 , and R_3 given by Eqs. (7)–(9) with respect to the relevant magnetic field h_H gives the following formula for the magnetization of

the Heisenberg spins of the IHM-THL:

$$\begin{aligned} m_H &= \frac{1}{24} \left[\frac{W_1}{V_1} + \frac{W_2}{V_2} + 3 \frac{W_3}{V_3} + 3 \frac{W_4}{V_4} \right] \\ &+ \frac{m_{\text{eff}}}{4} \left[\frac{W_1}{V_1} - \frac{W_2}{V_2} + \frac{W_3}{V_3} - \frac{W_4}{V_4} \right] \\ &+ \frac{\varepsilon_{\text{eff}}}{2} \left[\frac{W_1}{V_1} + \frac{W_2}{V_2} - \frac{W_3}{V_3} - \frac{W_4}{V_4} \right] \\ &+ \frac{\tau_{\text{eff}}}{3} \left[\frac{W_1}{V_1} - \frac{W_2}{V_2} - 3 \frac{W_3}{V_3} + 3 \frac{W_4}{V_4} \right], \end{aligned} \quad (17)$$

where the newly defined functions W_1 , W_2 , W_3 , and W_4 entering into Eq. (17) are given in Appendix B.

To complete an exact calculation of the single-site magnetization of the Heisenberg spins for the IHM-THL, it is just necessary to determine the pair and triplet correlation functions of the effective spin-1/2 Ising model on a triangular Husimi lattice, which can be also calculated within the framework of exact recursion relations [21] by following the same steps as previously used for a zero-field limit of the investigated model system [52]. The exact results for the pair and triplet correlation functions ε_{eff} and τ_{eff} can be, consequently, written

in this compact form

$$\varepsilon_{\text{eff}} = \langle \sigma_i^z \sigma_j^z \rangle_{\text{eff}} = \frac{1}{4} \left[\frac{\exp(\beta R_1) \omega - v x^{q-1}}{\exp(\beta R_1) + x^q} \right], \quad (18)$$

$$\tau_{\text{eff}} = \langle \sigma_i^z \sigma_j^z \sigma_k^z \rangle_{\text{eff}} = \frac{1}{8} \left(\frac{\exp(\beta R_1) y - z x^{q-1}}{\exp(\beta R_1) + x^q} \right), \quad (19)$$

which are expressed in terms of the newly defined parameters ω , v , y and z given in Appendix B.

In this way, we have completed also the exact calculation of the single-site magnetization of the Heisenberg spins of the IHM-THL. Last but not least, one may proceed to a straightforward calculation of the total magnetization per one spin, which can be expressed through the previously calculated single-site magnetizations of the Ising and Heisenberg spins m_I and m_H according to the formula,

$$m_T = (m_I + q m_H)/(1 + q). \quad (20)$$

It is noteworthy that the formula (20) correctly takes into account the total number of the Ising (N) and Heisenberg (Nq) spins within a triangulated Husimi lattice with the ramification number q .

III. RESULTS AND DISCUSSION

In this section, we will proceed to a discussion of the most interesting results for the ground state and magnetization curves of the IHM-THL by considering the particular case with the ramification number $q = 2$, which mimics a magnetic structure of the polymeric coordination compounds $\text{Cu}_9\text{X}_2(\text{cpa})_6 \cdot n\text{H}_2\text{O}$ commonly referred to as a triangulated kagome lattice [37–39]. It is worthwhile to recall that the magnetic properties of the spin-1/2 Ising-Heisenberg model on triangulated kagome [48,49] and related Husimi [52,53] lattices at zero as well as nonzero temperatures were, up to now, comprehensively studied just at a zero magnetic field, whereas the effect of the external magnetic field upon its magnetic properties was examined just for a triangulated kagome lattice at zero temperature yet [49]. The readers interested in further details concerned with the magnetic behavior of the IHM-THL in the zero magnetic field are referred to our previous study [52]. However, it should be, nevertheless, mentioned that the IHM-THL with the particular value of the ramification number $q = 2$ displays either a ferromagnetic (for $J_I > 0$) or a ferrimagnetic (for $J_I < 0$) long-range order with nonzero spontaneous magnetization at sufficiently low temperatures in the parameter space $J_H/|J_I| > -2/3$, whereas the frustrated parameter region $J_H/|J_I| < -2/3$ supports the existence of a disordered spin-liquid phase with zero spontaneous magnetization at all temperatures. In what follows, we will, therefore, examine, in detail, the magnetization curves of the spin-1/2 Ising-Heisenberg model on a related triangulated Husimi lattice at nonzero temperatures and may bring new insights into low-temperature magnetization curves of the polymeric complexes $\text{Cu}_9\text{X}_2(\text{cpa})_6 \cdot n\text{H}_2\text{O}$ [40–43]. To reduce the number of free parameters, a strength of the Ising coupling constant $|J_I|$ will, henceforth, serve as an energy unit when defining two dimensionless parameters $k_B T/|J_I|$, $J_H/|J_I|$, and $h/|J_I|$ ($h \equiv h_I = h_H$) measuring a relative size of temperature, interaction ratio, and magnetic field, respectively.

A. Antiferromagnetic Ising coupling $J_I < 0$

Our attention will be, at first, devoted to the ground state and magnetization process of the IHM-THL with the ramification number $q = 2$ and the antiferromagnetic Ising coupling $J_I < 0$. Under this assumption, one may find five different ground states, which can be classified as

- (1) the classical ferrimagnetic phase |I),

$$|I\rangle = \prod_{k,j} |\downarrow\downarrow\downarrow\rangle_{\sigma_{k,j}} \otimes |\uparrow\uparrow\uparrow\rangle_{S_{k,j}}, \quad (21)$$

- (2) the classical ferromagnetic phase |II),

$$|II\rangle = \prod_{k,j} |\uparrow\uparrow\uparrow\rangle_{\sigma_{k,j}} \otimes |\uparrow\uparrow\uparrow\rangle_{S_{k,j}}, \quad (22)$$

- (3) the up-up-up (uuu) dimerized phase |III),

$$|III\rangle = \prod_{k,j} |\uparrow\uparrow\uparrow\rangle_{\sigma_{k,j}} \otimes \left\{ \begin{array}{l} \frac{1}{\sqrt{2}}(|\uparrow\downarrow\downarrow\rangle - |\downarrow\uparrow\downarrow\rangle)_{S_{k,j}}, \\ \frac{1}{\sqrt{2}}(|\downarrow\uparrow\downarrow\rangle - |\downarrow\downarrow\uparrow\rangle)_{S_{k,j}}. \end{array} \right. \quad (23)$$

- (4) the up-up-down (uud) trimerized phase |IV),

$$|IV\rangle = \prod_{k,j} |\uparrow\uparrow\downarrow\rangle_{\sigma_{k,j}} \otimes \left[\cos \alpha |\uparrow\downarrow\uparrow\rangle - \frac{\sin \alpha}{\sqrt{2}} (|\uparrow\uparrow\downarrow\rangle + |\downarrow\uparrow\uparrow\rangle) \right]_{S_{k,j}}, \quad (24)$$

- (5) the up-up-up (uuu) dimerized ground-state |V),

$$|V\rangle = \prod_{k,j} |\uparrow\uparrow\uparrow\rangle_{\sigma_{k,j}} \otimes \left\{ \begin{array}{l} \frac{1}{\sqrt{2}}(|\uparrow\downarrow\uparrow\rangle - |\downarrow\uparrow\uparrow\rangle)_{S_{k,j}}, \\ \frac{1}{\sqrt{2}}(|\uparrow\uparrow\downarrow\rangle - |\uparrow\downarrow\uparrow\rangle)_{S_{k,j}}. \end{array} \right. \quad (25)$$

Note that the eigenvectors (21)–(25) are written as a tensor product of two state vectors, whereas the former (latter) state vector determines spin orderings of three Ising spins $\sigma_{k,j}$ (Heisenberg spins $S_{k,j}$) from the k th triangle-in-triangles unit described by the cluster Hamiltonian (3). The mixing angle determining probability amplitudes within the uud trimerized ground-state |IV) is given by $\alpha = \frac{1}{2} \arctan\left(\frac{\sqrt{8}J_H}{J_H+2J_I}\right)$. For better illustration, the relevant spin arrangements of the triangle-in-triangles units pertinent to the individual ground-states (21)–(25) are schematically visualized in Fig. 4 and will be described in a more detail below. The overall ground-state phase diagram is plotted in Fig. 5 on the $J_H/|J_I| - h/|J_I|$ plane, whereas analytical expressions for depicted ground-state

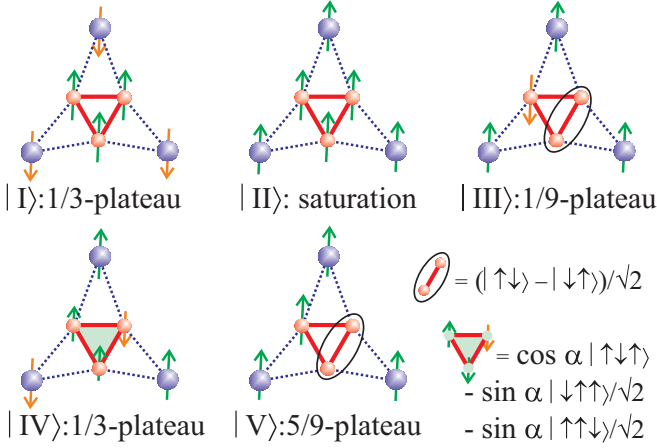


FIG. 4. Typical spin arrangements of one triangle-in-triangles unit within five available ground states (21)–(25) of the IHM-THL with the ramification number $q = 2$: the classical ferrimagnetic phase [I], the classical ferromagnetic phase [II], the uuu dimerized phase [III], the uuu trimerized phase [IV], and the uuu dimerized state [V]. An oval stands for a dimer-singlet state, whereas a trimerized state involving a quantum superposition of three uud states is marked by a shaded triangle.

phase boundaries read as follows:

$$\text{I/II: } \frac{h}{|J_I|} = 2,$$

$$\text{I/III: } \frac{h}{|J_I|} = -2 - 3 \frac{J_H}{|J_I|},$$

$$\text{I/IV: } \frac{J_H}{|J_I|} = -\frac{4}{5},$$

$$\text{I/V: } \frac{h}{|J_I|} = 4 + 3 \frac{J_H}{|J_I|},$$

$$\text{II/V: } \frac{h}{|J_I|} = 1 - \frac{3}{2} \frac{J_H}{|J_I|},$$

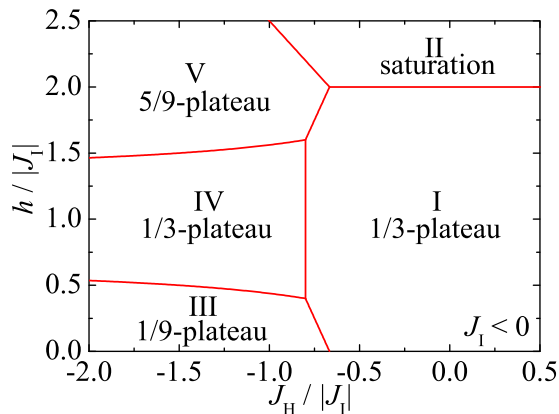


FIG. 5. The ground-state phase diagram of the IHM-THL on the $J_H/|J_I| - h/|J_I|$ plane established by considering the antiferromagnetic Ising coupling $J_I < 0$.

$$\text{III/IV: } \frac{h}{|J_I|} = 1 - \frac{3}{2} \frac{J_H}{|J_I|} - \sqrt{\left(1 - \frac{1}{2} \frac{J_H}{|J_I|}\right)^2 + 2 \left(\frac{J_H}{|J_I|}\right)^2},$$

$$\text{IV/V: } \frac{h}{|J_I|} = 1 + \frac{3}{2} \frac{J_H}{|J_I|} + \sqrt{\left(1 - \frac{1}{2} \frac{J_H}{|J_I|}\right)^2 + 2 \left(\frac{J_H}{|J_I|}\right)^2}.$$

It is evident that the first two classical ground-states [I] and [II] differ just in a relative orientation of the Ising and Heisenberg spins, which are contrarily aligned within the classical ferrimagnetic phase (21) and equally aligned within the classical ferromagnetic phase (22). These classical phases emerge as the respective ground states predominantly in the parameter region with the ferromagnetic ($J_H/|J_I| > 0$) or weak antiferromagnetic ($J_H/|J_I| \lesssim 0$) character of the Heisenberg coupling in accordance with the ground-state phase diagram (see Fig. 5). The antiparallel alignment of the Ising and Heisenberg spins detected within the classical ferrimagnetic phase (21) originates from the antiferromagnetic Ising interaction $J_I < 0$, and it should manifest itself in the zero-temperature magnetization curve as an intermediate 1/3 plateau when the total magnetization is scaled with respect to the saturation magnetization. At high enough magnetic fields, the total magnetization naturally reaches full saturation due to a perfect alignment of all Ising and Heisenberg spins into a direction of the external magnetic field within the classical ferromagnetic phase (22).

A much more intriguing situation appears whenever a geometric spin frustration arising out from the sufficiently strong antiferromagnetic Heisenberg interaction $J_H/|J_I| \ll 0$ comes into play. Under this condition, there appear another three ground-states [III], [IV], and [V], which are according to the respective eigenvectors (23)–(25) of purely quantum origin as the Heisenberg trimers are being subject to a quantum superposition of either two states (the uuu dimerized phases [III] and [V]) or three states (the uud trimerized phase [IV]). At lowest magnetic fields, the uuu dimerized phase [III] with a remarkable quantum superposition of the Heisenberg trimers constitutes the ground state in which two Heisenberg spins are being subject to a singlet pairing (23), and the third Heisenberg spin is oriented in opposite to the magnetic field with regard to the antiferromagnetic nature of the Ising coupling $J_I < 0$ with the fully polarized Ising spins. Note, furthermore, that there exist two linearly independent ways of the singlet pairing within each Heisenberg trimer of the uuu dimerized phase [III], which should be accordingly highly macroscopically degenerate. The uuu dimerized phase [III] manifests itself in zero-temperature magnetization curves as an intermediate 1/9 plateau, which is, in general, enlarged upon reinforcement of the antiferromagnetic Heisenberg coupling $J_H/|J_I|$.

At moderate magnetic fields, the ground state is formed by the uud trimerized phase [IV], which involves a quantum superposition of three uud states of the Heisenberg trimers surrounded by three enclosing Ising spins being in the similar but yet classical uud spin arrangement. It should be noted that the Ising spins, which are coupled to two Heisenberg spins with a local positive magnetization being subject to a quantum reduction of the magnetization, are aligned in opposite to the magnetic field with regard to the antiferromagnetic character

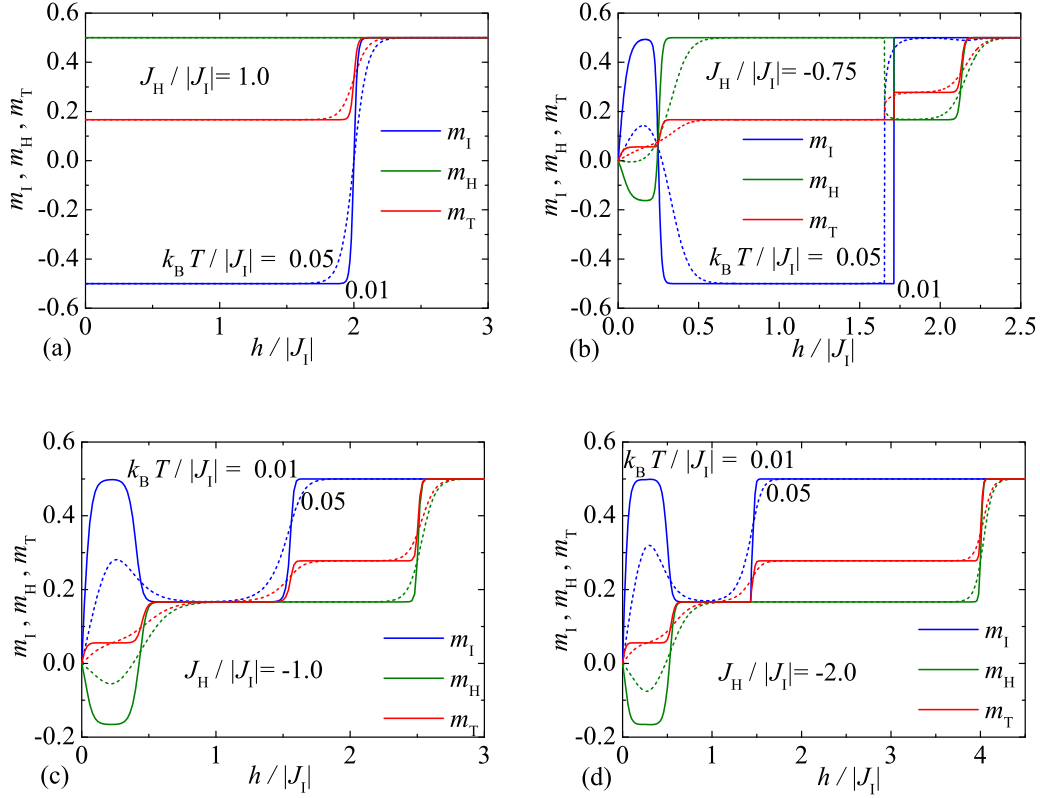


FIG. 6. Isothermal magnetization curves of the IHM-THL with the antiferromagnetic Ising coupling $J_I < 0$ at two different temperatures $k_B T/J_I = 0.01$ (solid lines) and 0.05 (dotted lines) when considering four different values of the interaction ratio: (a) $J_H/|J_I| = 1.0$; (b) $J_H/|J_I| = -0.75$; (c) $J_H/|J_I| = -1.0$; (d) $J_H/|J_I| = -2.0$. The single-site magnetization of the Ising (m_I) and Heisenberg (m_H) spins are plotted in addition to the total magnetization (m_T).

of the Ising coupling $J_I < 0$ (see Fig. 4 for a schematic illustration). The uud trimerized phase |IV) should be responsible in zero-temperature magnetization curves for the presence of another intermediate $1/3$ plateau, which is, however, of completely different origin as the intermediate $1/3$ plateau previously ascribed to the classical ferrimagnetic phase |I). The intermediate $1/3$ plateau due to the uud trimerized phase |IV) generally shrinks upon strengthening of the antiferromagnetic Heisenberg coupling $J_H/|J_I|$.

Last, but not least, one encounters at sufficiently high magnetic fields the other uuu dimerized phase |V), whose magnetic spin ordering is quite similar to the low-field uuu dimerized phase |III). As a matter of fact, all Ising spins are fully aligned towards the magnetic field, and there still exist two linearly independent ways of a singlet pairing (25) within each Heisenberg trimer of the uuu dimerized phase |V), which accordingly exhibits a high macroscopic degeneracy. The only difference with respect to the uuu dimerized phase |III) lies in that the third Heisenberg spin is in the uuu dimerized phase |V) polarized by the external magnetic field, which surpasses the effect of antiferromagnetic Ising coupling $J_I < 0$. The uuu dimerized phases |III) and |V), thus, differ from each other through the total spin of the Heisenberg trimers, which takes the value of $S_T^z = 1/2$ for the uuu dimerized phase |V) in contrast with the value of $S_T^z = -1/2$ present within the uuu dimerized phase |III). The uuu dimerized phase |V) should cause, in zero-temperature magnetization curves, existence of the intermediate $5/9$ plateau.

Now, a few comments are in order concerning with a direct comparison of the ground-state phase diagram of the IHM-THL with that one previously reported for the spin-1/2 Ising-Heisenberg model on a triangulated kagome lattice (cf. Fig. 5 with Fig. 9(a) from Ref. [49]). From this comparison, it is quite evident that the ground-state phase diagrams of both models are not only qualitatively similar, but also the nature of individual ground states is quite analogous. The zero-temperature magnetization curves of the IHM-THL should accordingly exhibit the completely same sequence of intermediate magnetization plateaus at $1/9$, $1/3$, and $5/9$ of the saturation magnetization as previously reported for the spin-1/2 Ising-Heisenberg model on a triangulated kagome lattice [49]. From this perspective, the IHM-THL captures well a physical mechanism behind the formation of the intermediate magnetization plateaus including their microscopic origin. However, the specific nature of the underlying triangulated Husimi lattice may be responsible for different degeneracies of some spin arrangements that might be a possible reason for small deviations in the respective magnetization curves at nonzero temperatures.

Let us corroborate the aforementioned ground-state analysis by a detailed examination of the low-temperature magnetization curves of the IHM-THL. To this end, the total magnetization is plotted in Fig. 6 against the magnetic field along with the single-site magnetizations of the Ising and Heisenberg spins at two different temperatures and four selected values of the interaction ratio $J_H/|J_I|$. Figure 6(a)

displays the low-temperature magnetization curve involving a single intermediate $1/3$ plateau, which is typically found for the particular cases with either ferromagnetic or weak antiferromagnetic Heisenberg coupling $J_H/|J_I| > -2/3$. Under this condition, the relevant results for the single-site magnetization of the Ising and Heisenberg spins are consistent with the spin arrangement of the classical ferrimagnetic phase (21) ascribed to the intermediate $1/3$ plateau.

On the other hand, the low-temperature magnetization curves of the IHM-THL with sufficiently strong antiferromagnetic Heisenberg coupling $J_H/|J_I| < -2/3$ are much more intricate because they involve three intermediate plateaus at $1/9$, $1/3$, and $5/9$ of the saturation magnetization [see Figs. 6(b)–6(d)]. If the antiferromagnetic Heisenberg coupling is of moderate strength $J_H/|J_I| \in (-4/5, -2/3)$, then, the first intermediate $1/9$ plateau corresponding to the uuu dimerized phase |III) is successively followed by the second intermediate $1/3$ plateau with the spin arrangement of the classical ferrimagnetic phase |I), whereas the third intermediate $5/9$ plateau is pertinent to the uuu dimerized phase |V). The single-site magnetizations of the Ising and Heisenberg spins depicted in Fig. 6(b) are in concordance with the aforementioned mechanism for the formation of the intermediate magnetization plateaus as well as with the established ground-state phase diagram shown in Fig. 5.

Although the low-temperature magnetization curves of the IHM-THL at stronger values of the antiferromagnetic Heisenberg coupling $J_H/|J_I| < -4/5$ still exhibit three intermediate plateaus at $1/9$, $1/3$, and $5/9$ of the saturation magnetization, it should be pointed out that the mechanism for the formation of the intermediate $1/3$ plateau is notably different from the previous case as it conforms with the uud trimerized phase |IV) instead of the classical ferrimagnetic phase |I) as the single-site magnetizations of the Ising as well as the Heisenberg spins are consistent with the uud spin arrangement [see Figs. 6(c) and 6(d)]. It also follows from Fig. 6 that the magnetization curves are substantially wiped out upon increasing of temperature, whereas the most narrow intermediate plateaus cannot be generally discerned in isothermal magnetization curves already at relatively low temperatures. As a matter of fact, any evident traces of the most tiny intermediate $1/9$ plateau are already absent in the isothermal magnetization curves plotted in Figs. 6(b)–6(d) for a relatively low temperature $k_B T/J_I = 0.05$.

B. Ferromagnetic Ising coupling $J_I > 0$

Next, we will examine in detail the ground state and magnetization process of the IHM-THL with the ramification number $q = 2$ and the ferromagnetic Ising coupling $J_I > 0$. The assumption of the ferromagnetic Ising coupling $J_I > 0$ substantially simplifies the ground-state analysis because the relevant ground state of the IHM-THL is either the classical ferromagnetic phase |II) for $h/J_I > -1 - 3J_H/(2J_I)$ or the uuu dimerized phase |V) for $h/J_I < -1 - 3J_H/(2J_I)$. From this perspective, the classical ferromagnetic phase |II) given by the eigenvector (22) is the ground state regardless of a relative size of the magnetic field h/J_I whenever the coupling ratio is greater than the threshold value $J_H/|J_I| > -2/3$. The only peculiar low-temperature magnetization process

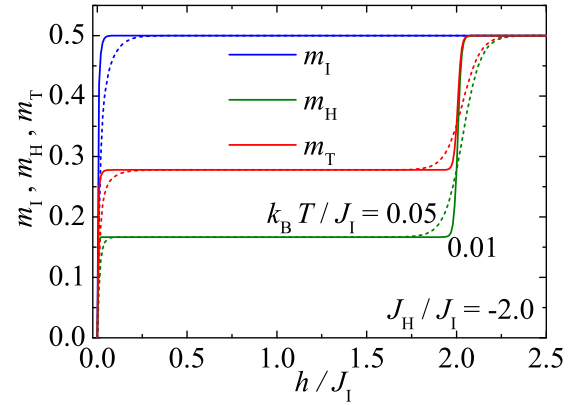


FIG. 7. Isothermal magnetization curves of the IHM-THL with the ferromagnetic Ising coupling $J_I > 0$ at two different temperatures $k_B T/J_I = 0.01$ (solid lines) and 0.05 (dotted lines) when assuming the interaction ratio $J_H/J_I = -2.0$. The single-site magnetization of the Ising (m_I) and Heisenberg (m_H) spins are plotted in addition to the total magnetization (m_T).

including the fractional intermediate plateau can be, thus, found just when a geometric spin frustration triggered by a sufficiently strong antiferromagnetic Heisenberg interaction $J_H/|J_I| < -2/3$ causes existence of the uuu dimerized phase |V) at low enough magnetic fields. To illustrate the case, we have depicted in Fig. 7 the isothermal magnetization curve of the IHM-THL by considering specific value of the interaction ratio $J_H/|J_I| = -2.0$. It actually turns out that the low-temperature magnetization curve displays, at sufficiently low magnetic fields, the intermediate $5/9$ plateau attributable to the uuu dimerized phase |V), which is characterized by a perfect alignment of the Ising spins into the magnetic field and a double degeneracy of a singlet pairing within each Heisenberg trimer of the uuu dimerized phase |V) as specified by the eigenvector (25).

IV. CONCLUSION

In the present paper, we have exactly solved the IHM-THL in a magnetic field by combining the generalized star-triangle mapping transformation with the method of exact recursion relations. It has been shown that the generalized star-triangle transformation establishes a rigorous mapping correspondence between the investigated model system and the spin-1/2 Ising model on a triangular Husimi lattice with the effective (temperature-dependent) field, pair, and triplet interactions. This latter effective model has been, subsequently, solved by the method of exact recursion relation in order to complete the relevant exact calculation for the IHM-THL.

Our particular attention has been, subsequently, focused on a detailed examination of the ground-state and low-temperature magnetization curves of the IHM-THL with the specific value of the ramification number $q = 2$, which is highly reminiscent of a triangulated kagome lattice experimentally detected in a series of the polymeric coordination compounds $\text{Cu}_9\text{X}_2(\text{cpa})_6 \cdot n\text{H}_2\text{O}$ [37–39]. Exact results obtained for the low-temperature magnetization curves of the IHM-THL indicate five different magnetization scenarios

depending on the character and relative size of both considered coupling constants.

It has been found that the low-temperature magnetization curves of the IHM-THL with the ferromagnetic Ising interaction $J_I > 0$ do not exhibit any intermediate plateau for $J_H/J_I > -2/3$ or they display just a single intermediate plateau at 5/9 of the saturation magnetization for $J_H/J_I < -2/3$. The situation is much more intricate for the IHM-THL with the antiferromagnetic Ising interaction $J_I < 0$, which shows a single intermediate plateau at 1/3 of the saturation magnetization for $J_H/J_I > -2/3$ or three different intermediate plateaus at 1/9, 1/3, and 5/9 of the saturation magnetization for $J_H/J_I < -2/3$. However, the mechanism for formation of the intermediate 1/3 plateau can still be quite different in the latter case: One either encounters, in a magnetization process, the classical ferrimagnetic phase |I) for $J_H/J_I > -4/5$ or the more peculiar uud trimerized phase |IV) for $J_H/J_I < -4/5$. It has been also argued that the intermediate 1/9 and 5/9 plateaus are macroscopic manifestations of the uuu dimerized phases |III) and |V), which involve according to the eigenvectors (23) and (25) within each Heisenberg trimer two linearly independent ways of a singlet pairing.

Last, but not least, it should be also mentioned that the intermediate plateaus should be clearly discernible also in high-field magnetization curves of triangulated kagome compounds $\text{Cu}_9\text{X}_2(\text{cpa})_6 \cdot n\text{H}_2\text{O}$ [37–39] recorded at sufficiently low temperatures, which makes out of this prominent class of highly frustrated magnetic materials attractive playground for a future experimental testing of unusual dimerized and trimerized quantum states of matter.

ACKNOWLEDGMENTS

This work was supported by the Slovak Research and Development Agency under Grant No. APVV-16-0186. The financial support provided by the VEGA Grant No. 1/0531/19 is also gratefully acknowledged.

APPENDIX A: THE EQUATIONS FOR ALL AVAILABLE ISING SPIN CONFIGURATIONS

The first two equations are obtained for two uniform configurations with three equally aligned Ising spins pointing up $\uparrow\uparrow\uparrow$,

$$\begin{aligned} V_1 &= 2 \exp\left(\frac{3}{4}\beta J_H\right) \cosh\left[\frac{3}{2}\beta(J_I + h_H)\right] \\ &+ 2 \exp\left(\frac{3}{4}\beta J_H\right) \cosh\left[\frac{\beta}{2}(J_I + h_H)\right] \\ &+ 4 \exp\left(-\frac{3}{4}\beta J_H\right) \cosh\left[\frac{\beta}{2}(J_I + h_H)\right] \\ &= A \exp\left(\frac{3}{4}\beta R_2 + \frac{1}{8}\beta R_3 + \frac{3\beta R_1}{2q}\right), \end{aligned} \quad (\text{A1})$$

or down $\downarrow\downarrow\downarrow$,

$$\begin{aligned} V_2 &= 2 \exp\left(\frac{3}{4}\beta J_H\right) \cosh\left[\frac{3}{2}\beta(J_I - h_H)\right] \\ &+ 2 \exp\left(\frac{3}{4}\beta J_H\right) \cosh\left[\frac{\beta}{2}(J_I - h_H)\right] \\ &+ 4 \exp\left(-\frac{3}{4}\beta J_H\right) \cosh\left[\frac{\beta}{2}(J_I - h_H)\right] \\ &= A \exp\left(\frac{3}{4}\beta R_2 - \frac{1}{8}\beta R_3 - \frac{3\beta R_1}{2q}\right), \end{aligned} \quad (\text{A2})$$

whereas another two equations are obtained for six nonuniform configurations with one Ising spin pointing in opposite with respect to the other, i.e., for three Ising spin configurations of type $\uparrow\uparrow\downarrow$,

$$\begin{aligned} V_3 &= 2 \exp\left(\frac{3}{4}\beta J_H\right) \cosh\left[\frac{\beta}{2}(J_I + 3h_H)\right] \\ &+ 2 \exp\left(-\frac{3}{4}\beta J_H\right) \cosh\left[\frac{\beta}{2}(J_I + h_H)\right] \\ &+ 2 \exp\left(\frac{\beta h_H}{2}\right) \cosh\left(\frac{1}{2}\beta Q^+\right) \\ &+ 2 \exp\left(-\frac{\beta h_H}{2}\right) \cosh\left(\frac{1}{2}\beta Q^-\right) \\ &= A \exp\left(-\frac{\beta R_2}{4} - \frac{1}{8}\beta R_3 + \frac{\beta R_1}{2q}\right), \end{aligned} \quad (\text{A3})$$

and three Ising spin configurations of type $\uparrow\downarrow\downarrow$,

$$\begin{aligned} V_4 &= 2 \exp\left(\frac{3}{4}\beta J_H\right) \cosh\left[\frac{\beta}{2}(J_I - 3h_H)\right] \\ &+ 2 \exp\left(-\frac{3}{4}\beta J_H\right) \cosh\left[\frac{\beta}{2}(J_I - h_H)\right] \\ &+ 2 \exp\left(\frac{\beta h_H}{2}\right) \cosh\left(\frac{1}{2}\beta Q^-\right) \\ &+ 2 \exp\left(-\frac{\beta h_H}{2}\right) \cosh\left(\frac{1}{2}\beta Q^+\right) \\ &= A \exp\left(-\frac{\beta R_2}{4} + \frac{1}{8}\beta R_3 - \frac{\beta R_1}{2q}\right). \end{aligned} \quad (\text{A4})$$

The Boltzmann weights (A3) and (A4) are expressed in terms of the parameters Q^\pm defined as follows:

$$Q^\pm = \sqrt{\left(\frac{J_H}{2} \pm J_I\right)^2 + 2J_H^2}. \quad (\text{A5})$$

**APPENDIX B: THE FUNCTIONS FOR CALCULATION
OF HEISENBERG MAGNETIZATION**

The functions W_1 , W_2 , W_3 , and W_4 entering into Eq. (17) are calculated as follows:

$$W_1 = 3 \exp\left(\frac{3}{4}\beta J_H\right) \sinh\left[\frac{3}{2}\beta(J_I + h_H)\right] + \exp\left(\frac{3}{4}\beta J_H\right) \sinh\left[\frac{\beta}{2}(J_I + h_H)\right] + 2 \exp\left(-\frac{3}{4}\beta J_H\right) \sinh\left[\frac{\beta}{2}(J_I + h_H)\right], \quad (\text{B1})$$

$$W_2 = -3 \exp\left(\frac{3}{4}\beta J_H\right) \sinh\left[\frac{3}{2}\beta(J_I - h_H)\right] - \exp\left(\frac{3}{4}\beta J_H\right) \sinh\left[\frac{\beta}{2}(J_I - h_H)\right] - 2 \exp\left(-\frac{3}{4}\beta J_H\right) \sinh\left[\frac{\beta}{2}(J_I - h_H)\right], \quad (\text{B2})$$

$$W_3 = 3 \exp\left(\frac{3}{4}\beta J_H\right) \sinh\left[\frac{\beta}{2}(J_I + 3h_H)\right] + \exp\left(-\frac{3}{4}\beta J_H\right) \sinh\left[\frac{\beta}{2}(J_I + h_H)\right] + \exp\left(\frac{\beta h_H}{2}\right) \cosh\left(\frac{1}{2}\beta Q^+\right) - \exp\left(-\frac{\beta h_H}{2}\right) \cosh\left(\frac{1}{2}\beta Q^-\right), \quad (\text{B3})$$

$$W_4 = -3 \exp\left(\frac{3}{4}\beta J_H\right) \sinh\left[\frac{\beta}{2}(J_I - 3h_H)\right] - \exp\left(-\frac{3}{4}\beta J_H\right) \sinh\left[\frac{\beta}{2}(J_I - h_H)\right] + \exp\left(\frac{\beta h_H}{2}\right) \cosh\left(\frac{1}{2}\beta Q^-\right) - \exp\left(-\frac{\beta h_H}{2}\right) \cosh\left(\frac{1}{2}\beta Q^+\right). \quad (\text{B4})$$

The parameters ω , v , y , and z are given as follows:

$$\omega = \frac{\exp(2\beta R_1 + \beta R_2 + \frac{\beta R_3}{4}) - \exp(\frac{\beta R_3}{4})x^{2q-2}}{\exp(2\beta R_1 + \beta R_2 + \frac{\beta R_3}{4}) + 2 \exp(\beta R_1)x^{q-1} + \exp(\frac{\beta R_3}{4})x^{2q-2}}, \quad (\text{B5})$$

$$v = \frac{\exp(2\beta R_1) - \exp(\beta R_2)x^{2q-2}}{\exp(2\beta R_1 + \beta R_2 + \frac{\beta R_3}{4}) + 2 \exp(\beta R_1)x^{q-1} + \exp(\frac{\beta R_3}{4})x^{2q-2}}, \quad (\text{B6})$$

$$y = \frac{\exp(2\beta R_1 + \beta R_2 + \frac{\beta R_3}{4}) - 2 \exp(\beta R_1)x^{q-1} + \exp(\frac{\beta R_3}{4})x^{2q-2}}{\exp(2\beta R_1 + \beta R_2 + \frac{\beta R_3}{4}) + 2 \exp(\beta R_1)x^{q-1} + \exp(\frac{\beta R_3}{4})x^{2q-2}}, \quad (\text{B7})$$

$$z = \frac{\exp(2\beta R_1) - 2 \exp(\beta R_1 + \frac{\beta R_3}{4})x^{q-1} + \exp(\beta R_2)x^{2q-2}}{\exp(2\beta R_1 + \beta R_2 + \frac{\beta R_3}{4}) + 2 \exp(\beta R_1)x^{q-1} + \exp(\frac{\beta R_3}{4})x^{2q-2}}. \quad (\text{B8})$$

-
- [1] C. Lhuillier and G. Misguich, in *High Magnetic Fields*, edited by C. Berthier, L. P. Lévy, and G. Martinez, Lecture Notes in Physics Vol. 595 (Springer, Berlin, 2001).
- [2] G. Misguich, C. Lhuillier, in *Frustrated Spin Systems*, edited by H. T. Diep (World Scientific, Singapore, 2004).
- [3] J. Richter, J. Schulenburg, A. Honecker, in *Quantum Magnetism*, edited by U. Schollwöck, J. Richter, D. J. J. Farnell, and R. F. Bishop, Lecture Notes in Physics Vol. 645 (Springer, Berlin, 2004).
- [4] C. Lacroix, P. Mendels, and F. Mila, *Introduction to Frustrated Magnetism*, (Springer, Berlin, 2011).
- [5] A. Honecker, *J. Phys.: Condens. Matter* **11**, 4697 (1999).
- [6] A. Honecker, J. Schulenburg, and J. Richter, *J. Phys.: Condens. Matter* **16**, S749 (2004).
- [7] F. Heidrich-Meisner, I. A. Sergienko, A. E. Feiguin, and E. R. Dagotto, *Phys. Rev. B* **75**, 064413 (2007).
- [8] H. Kageyama, K. Yoshimura, R. Stern, N. V. Mushnikov, K. Onizuka, M. Kato, K. Kosuge, C. P. Slichter, T. Goto, and Y. Ueda, *Phys. Rev. Lett.* **82**, 3168 (1999).
- [9] K. Onizuka, H. Kageyama, Y. Narumi, K. Kindo, Y. Ueda, and T. Goto, *J. Phys. Soc. Jpn.* **69**, 1016 (2000).
- [10] H. Kageyama, Y. Narumi, K. Kindo, K. Onizuka, Y. Ueda, and T. Goto, *J. Alloys Compd.* **317-318**, 177 (2001).
- [11] S. E. Sebastian, N. Harrison, P. Sengupta, C. D. Batista, S. Francoual, E. Palm, T. Murphy, N. Marcano, H. A. Dabkowska, and B. D. Gaulin, *Proc. Natl. Acad. Sci. USA* **105**, 20157 (2008).
- [12] Y. H. Matsuda, N. Abe, S. Takeyama, H. Kageyama, P. Corboz, A. Honecker, S. R. Manmana, G. R. Foltin, K. P. Schmidt, and F. Mila, *Phys. Rev. Lett.* **111**, 137204 (2013).
- [13] H. Tanaka, T. Ono, H. Aruga Katori, H. Mitamura, F. Ishikawa, and T. Goto, *Prog. Theor. Phys. Suppl.* **145**, 101 (2002).
- [14] T. Ono, H. Tanaka, H. Aruga Katori, F. Ishikawa, H. Mitamura, and T. Goto, *Phys. Rev. B* **67**, 104431 (2003).
- [15] Y. Narumi, Z. Honda, K. Katsumata, J.-C. Dömege, P. Sindzingre, C. Lhuillier, A. Matsuo, K. Suga, and K. Kindo, *J. Magn. Magn. Mater.* **272-276**, 878 (2004).

- [16] R. Okuma, D. Nakamura, T. Okubo, A. Miyake, A. Matsuo, K. Kindo, M. Tokunaga, N. Kawashima, S. Takeyama, and Z. Hiroi, *Nat. Commun.* **10**, 1229 (2019).
- [17] H. J. Liao, Z. Y. Xie, J. Chen, X. J. Han, H. D. Xie, B. Normand, and T. Xiang, *Phys. Rev. B* **93**, 075154 (2016).
- [18] M. Kurata, R. Kikuchi, and T. Watari, *J. Chem. Phys.* **21**, 434 (1953).
- [19] S. Katsura and M. Takizawa, *Prog. Theor. Phys.* **51**, 82 (1974).
- [20] P. D. Gujrati, *Phys. Rev. Lett.* **74**, 809 (1995).
- [21] R. J. Baxter, *Exactly Solved Models in Statistical Mechanics*, (Academic, New York, 1982).
- [22] J. L. Monroe, *J. Stat. Phys.* **67**, 1185 (1992).
- [23] J. L. Monroe, *Physica A* **256**, 217 (1998).
- [24] A. Z. Akhayan, N. S. Ananikian, and S. K. Dallakian, *Phys. Lett. A* **242**, 111 (1998).
- [25] N. S. Ananikian, V. V. Hovhannisyan, and H. A. Lazaryan, *Int. J. Mod. Phys. B* **24**, 5913 (2010).
- [26] E. Jurčišinová and M. Jurčišin, *J. Stat. Phys.* **147**, 1077 (2012).
- [27] E. Jurčišinová, M. Jurčišin, and A. Bobák, *Phys. Lett. A* **377**, 2712 (2013).
- [28] E. Jurčišinová, M. Jurčišin, and A. Bobák, *J. Stat. Phys.* **154**, 1096 (2014).
- [29] R. Huang and C. Chong, *J. Phys. Soc. Jpn.* **83**, 123002 (2014).
- [30] E. Jurčišinová and M. Jurčišin, *Physica A* **486**, 296 (2017).
- [31] E. Jurčišinová and M. Jurčišin, *Phys. Rev. E* **97**, 052129 (2018).
- [32] E. Jurčišinová and M. Jurčišin, *Physica A* **521**, 330 (2019).
- [33] M. E. Fisher, *Phys. Rev.* **113**, 969 (1959).
- [34] I. Syozi, *Phase Transition and Critical Phenomena*, edited by C. Domb and M. S. Green, (Academic, New York, 1972), Vol. 1, pp. 269–329.
- [35] O. Rojas, J. S. Valverde, and S. M. de Sousa, *Physica A* **388**, 1419 (2009).
- [36] J. Strečka, *Phys. Lett. A* **374**, 3718 (2010).
- [37] R. E. Norman, N. J. Rose, and R. E. Stenkamp, *J. Chem. Soc.: Dalton Trans.*, 2905 (1987).
- [38] R. E. Norman and R. E. Stenkamp, *Acta Crystallogr., Sect. C: Cryst. Struct. Commun.* **46**, 6 (1990).
- [39] M. Gonzalez, F. Cervantes-Lee, and L. W. ter Haar, *Mol. Cryst. Liq. Cryst.* **233**, 317 (1993).
- [40] S. Maruti and L. W. ter Haar, *J. Appl. Phys.* **75**, 5949 (1994).
- [41] S. Ateca, S. Maruti, and L. W. ter Haar, *J. Magn. Magn. Mater.* **147**, 398 (1995).
- [42] M. Mekata, M. Abdulla, T. Asano, H. Kikuchi, T. Goto, T. Morishita, and H. Hori, *J. Magn. Magn. Mater.* **177-181**, 731 (1998).
- [43] M. Mekata, M. Abdulla, M. Kubota, and Y. Oohara, *Can. J. Phys.* **79**, 1409 (2001).
- [44] H. S. C. Hamilton, W. M. Farmer, S. F. Skinner, and L. W. ter Haar, *AIP Adv.* **8**, 055802 (2018).
- [45] W. M. Farmer, S. F. Skinner, and L. W. ter Haar, *AIP Adv.* **8**, 101404 (2018).
- [46] S. F. Skinner, R. A. Coro, W. M. Farmer, J. H. Lovett, J. C. Lupton, J. A. Moses, B. M. Ortolano, L. R. Reid, S. D. Richardson, J. D. Taylor, and L. W. ter Haar, *AIP Adv.* **9**, 035112 (2019).
- [47] S. F. Skinner and L. W. ter Haar, *AIP Adv.* **10**, 025025 (2020).
- [48] J. Strečka, L. Čanová, M. Jaščur, and M. Hagiwara, *Phys. Rev. B* **78**, 024427 (2008).
- [49] D. X. Yao, Y. L. Loh, E. W. Carlson, and M. Ma, *Phys. Rev. B* **78**, 024428 (2008).
- [50] J. Čisárová and J. Strečka, *Phys. Rev. B* **87**, 024421 (2013).
- [51] J. Čisárová, F. Michaud, F. Mila, and J. Strečka, *Phys. Rev. B* **87**, 054419 (2013).
- [52] J. Strečka and C. Ekiz, *Phys. Rev. E* **91**, 052143 (2015).
- [53] C. Ekiz and J. Strečka, *Acta Phys. Pol. A* **137**, 592 (2020).